Open Ceramics 8 (2021) 100176

Contents lists available at ScienceDirect

Open Ceramics

journal homepage: www.sciencedirect.com/journal/open-ceramics

Micro-cantilever testing of diamond - silicon carbide interfaces in silicon carbide bonded diamond materials produced by reactive silicon infiltration

J. Ast [a], B. Matthey [a], P. Herre [b], S. Höhn [a], M. Herrmann [a,*], S.H. Christiansen [a,b]

[a] Fraunhofer IKTS, Fraunhofer Institute for Ceramic Technologies and Systems, Germany
[b] Institut für Nanotechnologie und Korrelative Mikroskopie gGmbH (INAM gGmbH), Germany

ARTICLE INFO

Keywords:
Interface
Strength
Diamond
Silicon carbide
Micromechanical testing

ABSTRACT

SiC-bonded diamond materials produced by pressureless reactive infiltration of diamond preforms with silicon show high hardness and wear resistance. These properties are due to the relatively high diamond volume content of approximately 50 vol% and the mechanically strong interface between diamond and SiC. To determine the bending strength of individual interfaces between diamond and SiC, micro-cantilevers were prepared by focused ion beam milling at 13 grain boundaries and in-situ bending tests were carried out in a scanning electron microscope. The determined strength of cantilevers showing interface fracture was 10.4 ± 4.0 GPa. Fracture surfaces were analyzed to verify the fracture behavior and initiation. In addition to fracture at the interface diamond/SiC, fracture occurred inside the SiC grains and at the SiC/silicon interface at comparable strength values. The results prove the high diamond/SiC-interface bonding strength.

1. Introduction

There is a need of wear resistant materials with low friction coefficients in different wear applications like bearings, sealings, inliners, cutting tools or nozzles [1–4]. One class of such materials are reinforced ceramic materials. The wear behavior of ceramic composites with hard reinforcing particles like diamond or cubic boron nitride (cBN) depends essentially on the strength of the particle/matrix interface [5–11]. A low strength of the particle/matrix interface leads to a breaking out of particles under load resulting in a decreased wear resistance of the components [7–11]. In particular, the incorporation of small cubic boron nitride grains into the Si_3N_4-matrix led to wear that was even higher than for the unreinforced material due to the weak grain boundaries [11]. A stronger bonding to the Si_3N_4-matrix by Ti(C,N) or SiC layers on diamond or cBN led to a significant reduction of wear. At the same time, the fracture mode changed. While in the Si_3N_4 diamond composites without coating the fracture was essentially intergranular at the diamond-matrix interface, the fracture in the composites with coated diamonds was transgranular [10]. Similar reduction in wear due to firmer incorporation of cBN in Al_2O_3 was found in Refs. [12,13].

Diamond and cBN-reinforced composites that have not been produced under high pressure can form weak grain boundaries. This is due to the fact that cBN and diamond are not stable under these conditions [3,4,14,15]. Therefore, the cubic modifications can transform into the hexagonal phase at the particle surface. Graphite and hexagonal BN show layered structures with low bonding forces between layers. That is why controlling the phase transformation and the properties of the grain boundaries in diamond-reinforced composites is an essential factor for producing wear-resistant materials. There are several ways to achieve this:

- Short-term densification under pressure typically using spark plasma sintering (SPS/FAST). Due to the short sintering time, the transformation can be kinetically hindered. The use of coarse or coated diamonds helps to reduce graphitization. The use of reactive systems, e.g. silicon, are particularly favorable in order to convert at least partially the non-diamond carbon that forms into strong secondary phases. The densification temperatures must be lower than 1600–1650 °C even for relatively short sintering times to minimize graphitization [10,11,16–20].
- Chemical vapour infiltration of diamond preforms with Si precursors to form a SiC binder phase. This is done at lower temperatures, giving high stability of the diamond. However, the process is limited in terms of the thickness of the components and is relatively time-consuming [17,18].

* Corresponding author.
E-mail address: mathias.herrmann@ikts.fraunhofer.de (M. Herrmann).

https://doi.org/10.1016/j.oceram.2021.100176
Received 17 July 2021; Received in revised form 17 August 2021; Accepted 24 August 2021
Available online 27 August 2021

- Large-format, extremely wear-resistant diamond materials with a high diamond content (45–55 vol-%) can be produced by liquid phase infiltration [20–27]. In this process, diamond preforms are infiltrated by capillary forces at temperatures higher than the melting point of Si (1425 °C). The Si reacts with the carbon of the binder and the diamond particles to form cubic β-SiC. The outer dimensions of such components are almost constant. However, the Si reacts with an increase in volume relative to the starting carbon volume, i.e., the SiC grows into the pores and a low content of residual silicon <5 vol-% can be realized [20,26,27].

The material investigated in this work is also produced by infiltrating diamond preforms with liquid Si. It is characterized by interpenetrating three-dimensional networks of SiC and diamond (Fig. 1a).

The forming cubic β-SiC grows essentially heteroepitaxially on the {111}-planes of the diamond. The crystalline lattices of the SiC and diamond are rotated by 30° to minimize stresses. Additional stacking faults can form at the boundary layer between diamond and SiC [20,27]. Also, by means of transmission electron microscopy (TEM) and electron energy loss spectroscopy (EELS), graphite formation could not be clearly detected at these interfaces [20,27].

In addition, there are areas (Fig. 1d) consisting of nanocrystalline SiC and residual Si (n-SiC). These regions form especially at areas where different SiC crystals, which have grown laterally on the surface, collide, or at originally non-faceted and rough diamond surfaces [20,27]. These nanocrystalline SiC crystals also exhibit an orientation relationship to the diamond, but this is different from that of the large epitaxially grown SiC crystals [20,27].

Graphitic interlayers of 10–300 nm were detected for materials produced at higher infiltration temperatures and/or longer heat treatment time (several hours) [20,25,27]. Such interlayers lead to a reduction in hardness. TEM investigations showed that the graphite formed in this process has an orientation relationship to the diamond. The graphite layers are arranged perpendicularly to the interface [20,27,28].

Another detrimental effect on the interface strength originates from Al impurities in Si, which segregate at the interface and form the chemically less stable Al_4C_3 phase [29].

To estimate the strength, calculations of the energy of the diamond/SiC-interface were carried out recently by Clayton et al. [29]. These calculations showed complex interfaces with stacking faults in the SiC on the one hand and graphitic structures on the other. The average energy of the interface was calculated to be 0.84 J/m^2, which is considerably lower than diamond-diamond interfaces (5.3 J/m^2) and SiC–SiC (2.06 J/m^2) but higher than graphite (0.2 J/m^2).

In recent years, nanoindentation-based techniques for measuring mechanical properties at the microscopic level have been developed. Nanoindentation [30,31], micro-cantilever bending and fracture [32–36] as well as micropillar compression [37] and splitting methods [38] were investigated and continuously improved. Specimens are typically prepared by focused ion beam (FIB) milling and tests performed in scanning electron microscopes. This allows the assessment of hardness, strength, and fracture properties of individual grains as a function of crystal orientation or even specific grain boundaries. A comprehensive review on the deformation and fracture behavior of transition metal carbides was recently published by Naughton-Duszová et al. [39].

So far, only Zhang et al. [40] mentioned a measured strength value for the diamond/SiC grain boundary of about 700 MPa, while the interface contained graphite and aluminum carbide. A mean value for the tensile strength of the Si/SiC-interface in SiSiC materials of 4.3 ± 1.9 GPa was determined by the same authors [41]. Scott [42] determined a wide range of bending strength values (2.9–10.4 GPa) for diamond/-diamond interfaces in polycrystalline diamond materials produced by high pressure high temperature method.

Therefore, it is necessary to characterize the process-dependent mechanical properties of the diamond/SiC interface in order to understand the excellent wear behavior of these materials and allowing a comparison with other systems.

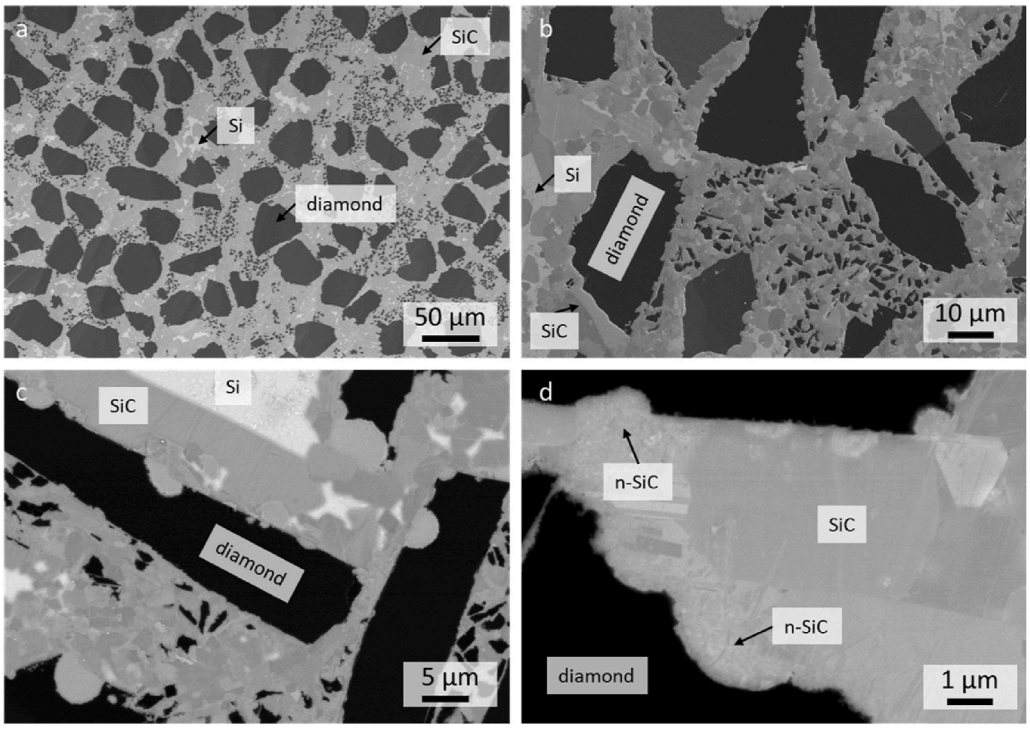

Fig. 1. FESEM micrographs showing the individual components of the SiC bonded diamond material: (a) overview, (b–d) higher magnifications of the various regions showing the distribution of residual silicon, diamond as well as larger SiC grains and nanocrystalline (n-SiC) areas in the vicinity of SiC-diamond interfaces.

2. Experimental

The silicon carbide bonded diamond composite was produced by silicon infiltration of pressed diamond preforms (dimensions 50 × 50 × 5 mm^3). The preform was prepared from bimodal diamond grain sizes of 50 µm (70 vol-%) and 5 µm. The details of production are described in Refs. [20,26,27]. The material has a density of 3.29 ± 0.02 g/cm^3. A diamond content of 49.3 ± 0.3 vol-% and a silicon content less than 5 vol-% were measured on a reference sample by image analysis of ion beam polished samples. The biaxial strength of the material measured on reference samples was 505 ± 40 MPa using the ball on three balls method [20].

The microstructure of the material is shown in Fig. 1. The orientation relationship between diamond and SiC was investigated using electron backscatter diffraction (EBSD). The measurements, which are shown in Fig. 2, were carried out using a Nordlys-detector (Oxford instruments Ltd.) in the same area as the subsequent micromechanical testing. The analysis of the orientation between diamond and silicon carbide in the actual sample reveals the same orientation relationship between diamond and 3C–SiC as observed in detailed investigations in Refs. [20,27]. The {111}-planes of the phases are parallel to each other with a rotation of 30° around (111) (Fig. 2).

The sample used for micromechanical analysis (of ~ 5 × 3 × 1 mm^3) was cut from a SiC bonded diamond plate (50 × 50 × 5 mm^3) using the CEPHEUS laser marking system from Photon Energy GmbH (Germany). The system is equipped with a pulsed Nd:VO_4 laser having a wavelength of 1064 nm and a pulse duration <15 ps. The laser cutting directions are indicated in Fig. 3a. Final surface polishing was carried out using a dedicated Ar^+ ion milling system (TIC3X, Leica Microsystems, Germany). A smooth surface was obtained after processing with 10 kV accelerating voltage and 3 mA Ar^+ ion current for approximately 24 h. It should be noted that due to the high hardness of the material, conventional mechanical grinding, sawing, and polishing techniques are inconvenient sample preparation procedures.

On the polished surface, 13 grain boundary areas between diamond and SiC were chosen and the cantilever beams were cut using FIB-machining (Ga^+ ions, 30 kV and 2–6 nA). The positions of the cantilevers are shown in Fig. 3b and c. The cross-section of the cantilever is pentagonal with an angle α of 35° (Fig. 4).

The bending tests were carried out in a FIB/SEM Crossbeam Auriga (Zeiss, Germany) with an integrated Alemnis nanoindentation system (Alemnis, Switzerland) using a cono-spherical diamond tip (Synton-MDP, Switzerland). A constant displacement rate of 10 nm/s was chosen for loading during the experiments until fracture occurred.

The bending stress σ_y at the top surface of the beam is calculated from the obtained load-displacement data using linear-elastic Euler-Bernoulli beam theory under the assumptions of an ideal pentagonal cross-section, a rigidly clamped beam and small displacements:

$$\sigma_y = \frac{F\,L}{I_y}\,a$$

$$I_y = \frac{BW^3}{12} + (a - W/2)^2\,BW + \frac{B^4}{288}(\tan\alpha)^3 + \left(\frac{B}{6}\tan\alpha + W - a\right)^2 \frac{B^2}{4}\tan\alpha$$

$$a = \frac{\frac{W^2}{2} + \frac{B}{4}\tan\alpha\left(W + \frac{B}{6}\right)}{W + \frac{B}{4}\tan\alpha}$$

where F is the load, L the lever arm, which is defined by the distance between the loading point and the location of failure initiation (in most but not all cases fracture occurred at the diamond-SiC interface), I_y -the second moment of area, a - the distance from the centroid C of the cross section, B and W dimensions of the cantilever cross-section (see Fig. 4).

3. Results

The load-displacement curves of the cantilevers are given in Fig. 5, the calculated strength values, which are given in Table 1, were calculated using the maximum force value before unstable failure. The data reveal that the displacement curves depend linearly on the load up to the fracture of the cantilever. Exceptions are the two cantilevers C2 and C11 (values in Table 1 in brackets), which do not show the catastrophic failure mode as the other samples but instead fail at considerably lower critical loads. The reason for this behavior is not completely clear. Intrinsic defects or sample preparation effects might cause the observed

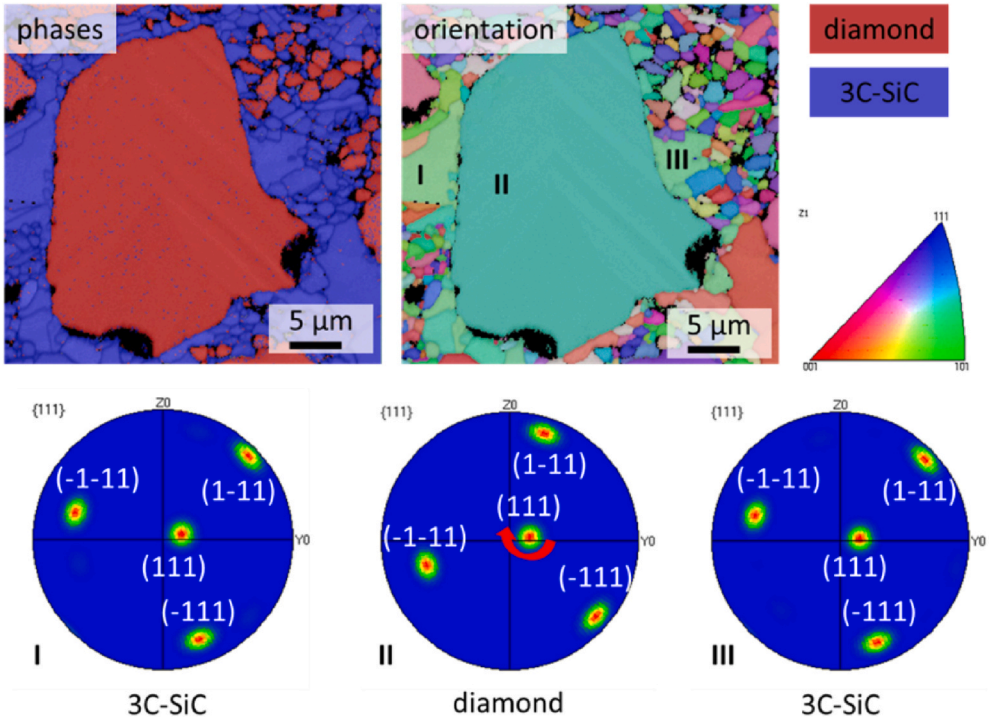

Fig. 2. Results of EBSD measurement of the composite. The analysis of the orientation between diamond and silicon carbide (region I, II and III) reveals a distinct orientation relationship. The {111}-planes are parallel to each other with a rotation of 30° around (111). This confirms the same orientation relationship between diamond and 3C–SiC in the actual sample as observed in detailed investigations in Refs. [20,27]. (For interpretation of the references to colour in this figure legend, the reader is referred to the Web version of this article.)

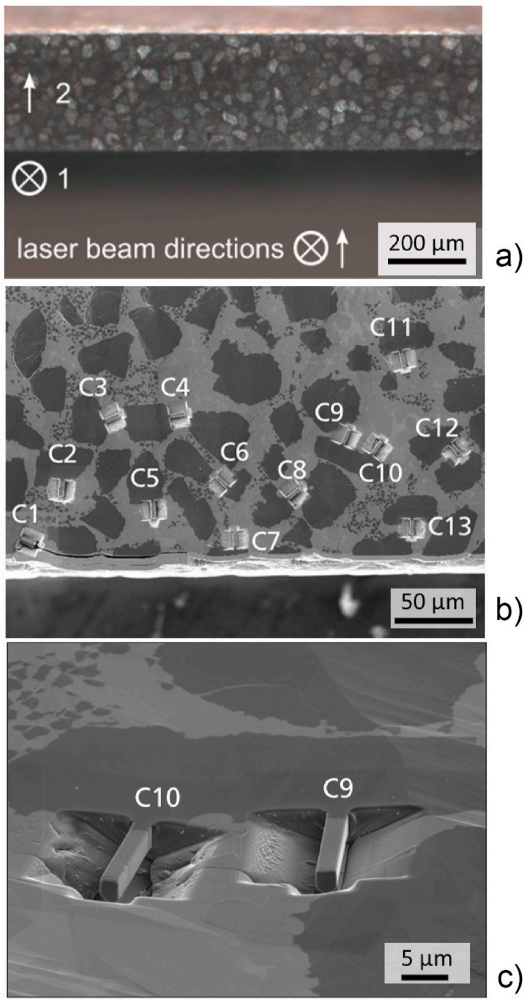

Fig. 3. Micrographs of the surface of the material (SiC (grey)//diamond (dark)) during sample preparation:
a) Light microscopy image after the initial sample preparation step by laser cutting. The consecutive cutting directions are indicated by the white cross and arrow,
b) SE overview image of the cantilevers (C1 – 13) cut at the interface by FIB,
c) Higher magnification SE image of cantilevers C9 and C10.

behavior at those interfaces.

Detailed fracture analysis was carried out after testing to visualize fracture surfaces and to understand the fracture initiation behavior. Some typical fracture surfaces are presented in Figs. 6–9. Based on the analysis, the fracture behavior could be divided into 3 classes:

- fracture at the interface diamond/SiC,
- fracture in SiC grains and
- fracture at the interface SiC/silicon.

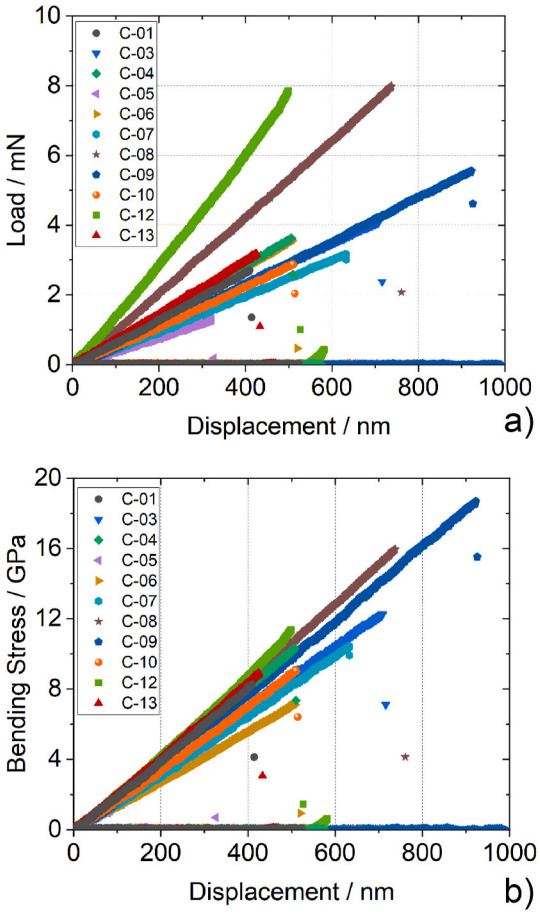

Fig. 5. Load-displacement (a) and stress-displacement curves (b) of the different beams.

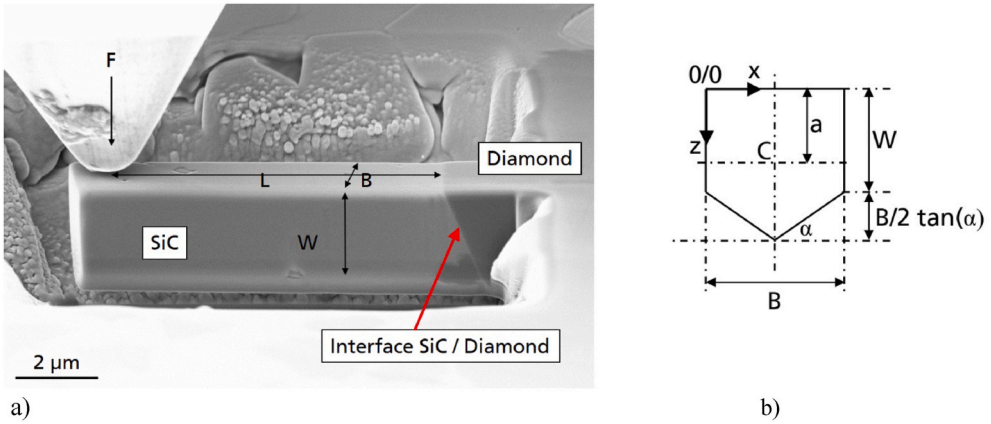

Fig. 4. a) SE image of a cantilever before loading. Important geometric dimensions are indicated within the image. The inclined interface between diamond and SiC is marked by a red arrow. b) sketch of the cantilever dimensions used for calculation of the area moment of inertia. The angle α was 35°.

Table 1
Calculated bending strength of the different cantilevers and the assignment to the observed fracture location (SiC/Diamond interface, SiC phase, Si/SiC interface) (1 - including C11; 2) – fracture origin not entirely obvious).

Cantilever	Strength, GPa		
	SiC/Diamond	SiC	Si/SiC
C1	8.3		
C2		(1.9)	
C3	12.3		
C4	10.4		
C5	4.9		
C6			7.2
C7	10.4		
C8		16.0[2)]	16.0[2)]
C9	18.6		
C10	9.1		
C11	(2.4)		
C12		11.4	
C13	8.90		
Mean	**10.4 (9.5)[1]**		
Standard Deviation	**4.0 (4.5) [1]**		

The classification is also shown in Table 1.

In Fig. 6 the fracture surface of cantilever C7 is shown. The fracture starts clearly at the interface. The SiC/diamond interface of cantilever 7 is straight indicating that it corresponds to a special orientation relation as shown in Fig. 2 and [20,27]. However, most of the fracture occurs not directly at the diamond surface but slightly in the SiC grain. This can be identified by the BSE contrast images acquired with an ESB (energy selective backscatter) detector (−1.0 kV grid voltage. 1.5 kV accelerating voltage) which is sensitive to the mean atomic number (Fig. 6 d). A very similar behavior was found also for the other specimens, which showed fracture at the SiC/diamond interface.

In Fig. 7 the fracture surface of cantilever C9 is shown. This interface is different from C7 as it exhibits a certain roughness, which is characteristic for interface regions consisting of nanocrystalline SiC in conjunction with residual Si (Fig. 1d) [20,27]. Most interestingly, it has the highest interfacial strength of 18.6 GPa. However, also in this case most of the fracture surface consists of SiC, i.e. the crack propagates in the SiC region near the interface.

Micrographs of tested cantilever C12 are given in Fig. 8. The fracture does not initiate at the interface diamond/SiC. but in the SiC grain approximately 700 nm away from the interface. However, the crack propagates partly along the diamond/SiC interface in the lower part of the cantilever.

The micrograph shows both kinds of interfaces: µm-sized SiC grains grown epitaxially on the diamond grain as well as an area consisting of nanocrystalline SiC (labeled as n-SiC).

A different behavior is depicted in Fig. 9 for cantilever C6. Here, the fracture did not take place at the interface diamond/SiC, but at the interface Si/SiC. The crack propagates through both phases, Si and SiC. This indicates that this interface must have a lower strength compared to the diamond/SiC interface at the root of the cantilever, where tensile stresses at the cantilever top side are even higher because of a larger bending moment. Also cantilever C8 (not shown here) did not fracture at the SiC/diamond interface but within the SiC. The micrographs reveal

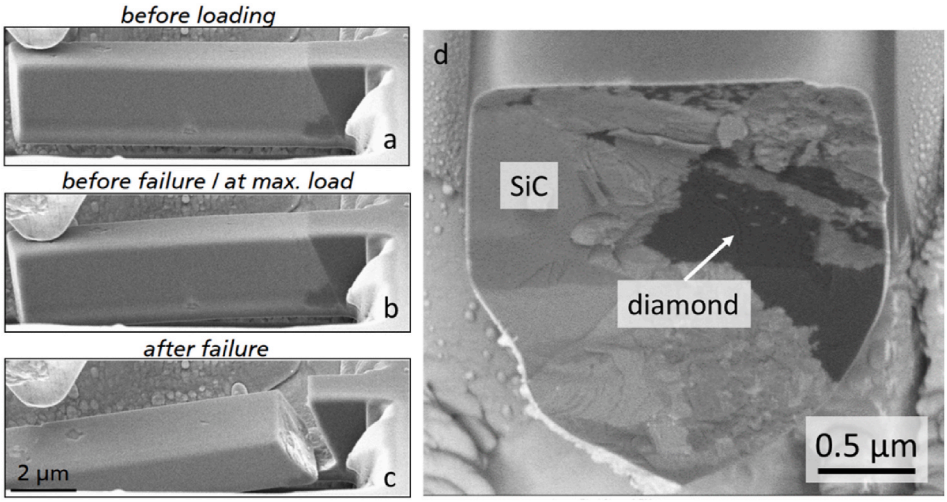

Fig. 6. SE micrograph sequence of cantilever C7(a–c) during the bending experiment. The fracture starts at the smooth diamond/SiC interface. However, most of the fracture occurs within the SiC and only partially at the diamond side as can be seen from the BSE image in (d).

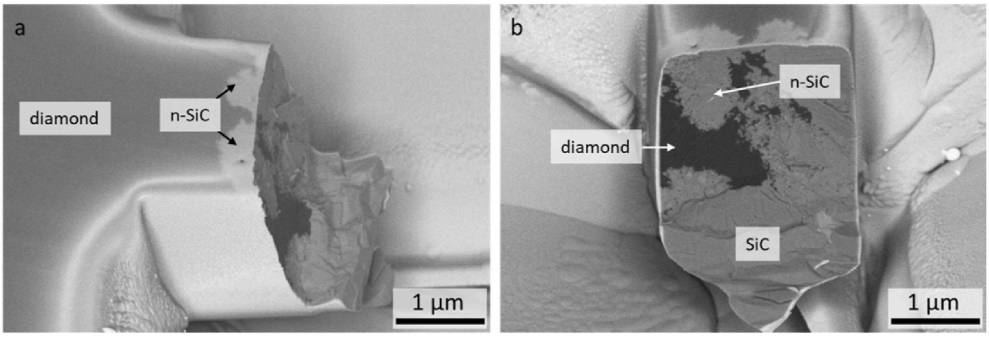

Fig. 7. BSE micrographs of tested cantilever C9. The fracture starts at the rough interface diamond/SiC consisting of nanocrystalline SiC (n-SiC, see also Fig. 1). However, most of the fracture occurs within the SiC area.

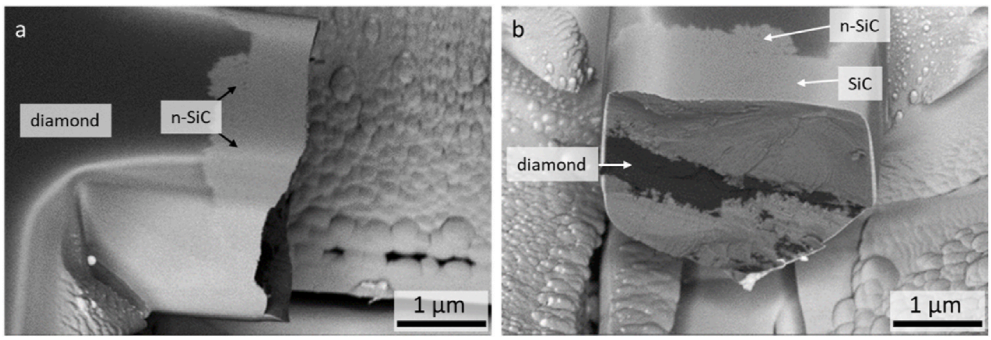

Fig. 8. BSE micrographs of tested cantilever C12. The fracture does not start at the interface diamond/SiC but within the SiC.

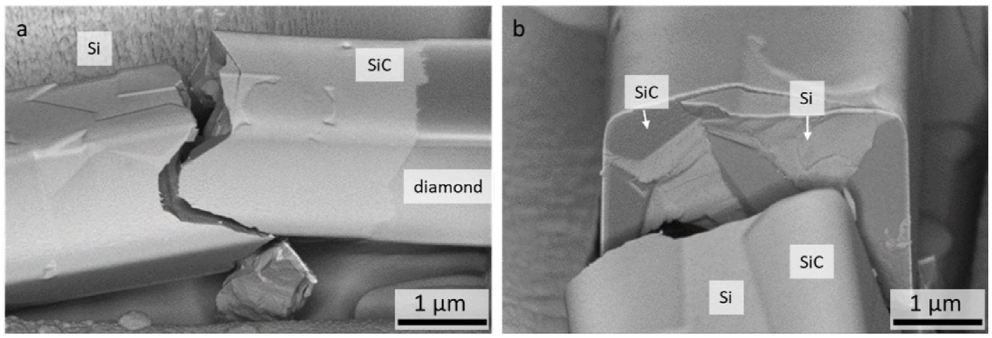

Fig. 9. BSE micrographs of tested cantilever C6. The fracture did not take place at the diamond/SiC interface, but at the interface Si/SiC.

small Si inclusions within the SiC phase at the fracture origin, which may act as fracture initiation sites due to stress concentrations or increased residual tensile stresses in the SiC.

4. Discussion

In literature there is still an ongoing discussion concerning the nature, composition, and properties of the interfaces in SiC bonded diamond materials produced by reactive infiltration. This is due to the facts, that.

- the preparation of the material takes place in nonequilibrium conditions. Therefore, graphite forms if adequate conditions for silicon infiltration are not selected resulting in changed interfacial properties and in the reduction of the hardness of the material [20,25,27]. The main factors influencing the graphitization are the infiltration temperature, time, and the purity of the material [25,27]. Our previous investigations have shown that no graphitization can be observed under the applied manufacturing conditions.
- impurities of Al or other metals seem to enrich at the interface to the diamond, resulting in Al_3C_4 or graphite formation. Both effects again reduce the strength of the interface [29]. Aluminum is beside iron and calcium a main natural contamination in technical silicon. So, with the use of silicon with a purity of 99.8 wt% the formation of Al_4C_3 precipitations can be prevented.

To the best of our knowledge no detailed experimental analysis of the strength of the diamond/SiC interface was carried out so far. Therefore, the data presented are important for the understanding of the performance of these materials.

The observed strength of the diamond/SiC interface of 10.4 ± 4.0 GPa (or 9.5 ± 4.5 GPa if the result of C11 is included) reveals a high interface strength, which is comparable to the values observed for diamond, diamond/diamond- [42], SiC/Si-interfaces [41] or the strength of WC [39] measured under similar conditions (Table 2).

Table 2
Comparison of the interfacial strength with literature data (1- Al carbide and graphite at the interface).

Interface	Method	Number of samples	Strength, GPa	Source
SiC/diamond	Bending	8	10.4 ± 4.0	This work
SiC/diamond	Bending		appr. 0.7[1)]	[40]
SiC/Si	Tension		4.3 + 1.9	[41]
Diamond grain	Bending	2	Between 7.4 and 12.2	[42]
Diamond/Diamond	Bending	4	7.1 ± 2.9 (max. value 10.4)	[42]
WC/WC grain boundary without special orientation	Bending	6	2.5–10	[39]
WC/WC grain boundary(CSL Σ = 2)	Bending	3	20–26	[39]
WC/Co/WC	Bending		2.5–4.5	[39]
			Grain boundary energy	
Diamond	MD calculations		5.3 J/m2	[43]
Graphite			0.2 J/m2	[43]
SiC/diamond			0.84 J/m2	[43]
SiC			2.33 J/m2	[43]

The cantilevers were all prepared under the same ion milling conditions and had approximately the same nominal dimensions. Slight differences in size such as length, width and cross sectional area were accounted for in the respective fracture mechanical equations and do not contribute to the observed variation between the strength values at failure. We, however, assume that the local phase composition, the inclination of the interface and the SiC-crystallite sizes all influence the interfacial strength and contribute to spatially varying stresses. These structural details determine the resulting maximum force values and

therefore the strength as measured by the individual cantilevers. Site specific in-situ tests, such as micro-cantilever testing in combination with high resolution scanning electron microscopy imaging allow to differentiate between all these effects, which originate from the local microstructure. This causes the observed variation in strength values but shows at the same time the importance of localized testing techniques as presented in this study.

In the publication of Naughton-Duszová et al. [39] the results on WC-Co materials determined under similar conditions were published for the interface strength of WC/WC as well as WC/Co grain boundaries. In this publication, it was shown that depending on the nature of the interface different values were observed. For low energy grain boundaries for example CSL ($\Sigma = 2$), higher bending strength could be observed in comparison to boundaries without special orientations.

Also, Scott [42] measured beside interfacial bending strengths of 7–10.4 GPa also low values of 2–3 GPa. The reason for this large gap was not completely clear.

High values were observed not only for the epitaxially grown interface, but also for rough interfaces containing nanocrystalline SiC and Si. This reveals, that also this type of interface shows high strength.

The observed values are more than 10 times higher than the published strength values of 700 MPa for graphite and Al carbide containing diamond/SiC-interfaces [40]. The difference is probably linked to the clean epitaxial grown interfaces in the here investigated material.

Based on the observation of the partial failure of the cantilevers at the Si/SiC interfaces or within the SiC, it is clear that the diamond/SiC-interface in this specimen must be as strong or even stronger than the Si/SiC interface. Whenever fracture occurred in the SiC phase or at the interface Si/SiC, the critical bending stress was lower than the bending stress acting at the interface diamond/SiC because the bending stress is the highest in the vicinity of the cantilever support where the SiC/diamond interfaces were placed.

Only two measured values are available for the Si/SiC-interface. Therefore, the interpretation must be made with caution. However, they seem to indicate similar strength levels as measured by Hsu et al. [41].

In [43] the fracture energy distributions of SiC, diamond/SiC-interfaces, diamond and graphite were calculated using Molecular Dynamics (MD)-calculations (Table 2). The mean value for diamond/SiC interfaces was calculated to be only 1/6 of the value of diamond and 1/3 of the values of SiC. In this context, our results suggest that these values are too low.

Simple geometrical considerations (assuming ball-like diamond particles; Fig. 10) and the experimentally observed complete transgranular fracture of diamond in the investigated material [20] suggest that the interfacial energy must be larger than ½ of the fracture energy of diamond, otherwise the crack along the interface would be energetically more favorable:

$$\gamma_{interface} 2\frac{\pi d^2}{2} > \gamma_{diamond} 2\frac{\pi d^2}{4}$$

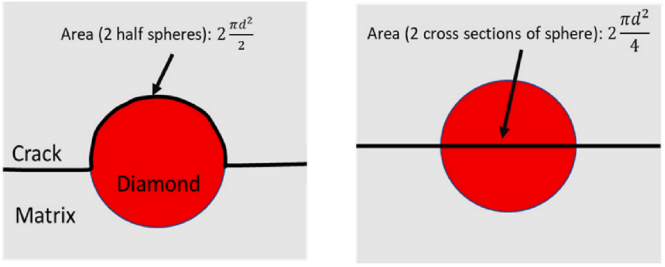

Fig. 10. Schematic view of the geometry of the intergranular and transgranular fracture.

$$\gamma_{interface} > \frac{\gamma_{diamond}}{2}$$

In the reported calculated interfacial structures [43] graphitic layers or clusters were observed, which were not found by TEM investigations in our material. This could be a reason for the observed differences. In addition, it must be noted that the boundary is formed in a kinetic mode. Once formed, Si–C bonds on the diamond surface are hard to break due to the high activation energy, which kinetically hampers a further transformation of the interface towards equilibrium.

Even if graphite directly forms at the interface, it grows epitaxially [20,27]. The inherently strong graphene sheets are oriented perpendicular to the interface. Therefore, the rupture of the interface means that the bonds inside the graphene sheets must be broken, which needs much more energy than the simple separation of the sheets (if graphene layers are parallel to the interface). The calculated interface energy of 0.2 J/m^2 in Ref. [43] corresponds to the case of separating graphene layers. The energy of bonds in the graphene layers is even higher than the C–C bonds in diamond. However, the density of bonds is lower.

It must be mentioned that the oxidation behavior of the material proved the existence of very local direct diamond/diamond contacts (size typical less than 1 μm), which were formed during the preform preparation [44]. At these local interfacial areas, the bond between the diamond consists only of glassy or graphite like carbon. These few contacts have probably low strength. However, their dimensions were only in the sub μm range and will not act as macroscopic defect sites but could influence the behavior on the microscale. This could be the reason for the observed low strength of cantilever 11.

The high strength of the bonding between SiC and diamond is also supported by the fact that the crack propagates mostly in the SiC and not directly at the interface. The crack deflects out of the interface which may be due to the SiC phase being under tension, while the diamond and silicon in these materials are under compression [45]. Furthermore, the stress in the micro-cantilevers is not homogeneously distributed since tensile stresses act at the top and continuously become compressive towards the lower beam side, passing through the neutral axis. Inclined and uneven interfaces may additionally alter the crack propagation behavior. Finally, formed stacking faults in the SiC may influence the kinetics of the crack propagation.

5. Conclusions

SiC-bonded diamond materials produced by pressureless reactive infiltration of diamond preforms with liquid Si show excellent hardness, wear resistance and high thermal conductivity. All these properties are essentially determined by the properties of the interface in addition to the high achievable diamond volume content of approx. 50 vol%. Depending on the conditions of silicon infiltration the composition, microstructure and properties of the interface can change. The material investigated here shows no significant precipitation of graphite at the grain boundaries, which are characterized by an epitaxial growth of the reactively formed SiC grains on diamond. In addition, there are areas with nanocrystalline SiC and residual silicon near the interface. No significant difference in strength was found for both types of grain boundary regions within the scatter range and the limited number of measured values (eight specimens). More extensive investigations may possibly lead to a distinction here. The determined value of 10.4 ± 4.0 GPa agrees well with those measured on polycrystalline diamond [42], indicating the high strength of the interface.

The strength values determined for the interface in this work show values similar to those found for the cantilevers broken in the SiC phase or at the SiC/Si interfaces.

All these data show that with an optimal manufacturing technology and purity of the material clean diamond-SiC interfaces can be reproducibly achieved in pressureless produced SiC bonded diamond materials, which are a key factor for preserving enhanced wear properties of

these materials.

Declaration of competing interest

The authors declare that they have no known competing financial interests or personal relationships that could have appeared to influence the work reported in this paper.

Acknowledgement

The sample preparation and microstructural analysis was supported by the Federal Ministry for Economic Affairs and Energy in the maritime research program under the project SUBSEASLIDE (contract number 03SX508F).

J.A. & S.H.C. acknowledge funding via the European Research Council (ERC) Synergy grant 4D-nanoSCOPE (grant no. 810316). Furthermore. P.H. & S.H.C. thank the Bavarian Ministry of Economic Affairs, Regional Development and Energy for financial support within the framework of the INAM research institute development.

References

[1] Deutsche Keramische Gesellschaft (DKG), Expertenstudie, in: Zukunftspotentiale von Hochleistungskeramiken. DKG: Köln. Germany, 2014, 978-3-00-045777-7, www.expertenstudie-hlk.dkg.de. (Accessed 20 May 2021). accessed on.

[2] Superhard Materials Market, 2025. Global market insights. Selbyville. Delaware 19975. USA. https://www.rnrmarketresearch.com/global-superhard-material-market-insights-forecast-to-2025-market-report.html, 2019. (Accessed 9 June 2021) accessed.

[3] R. Riedel (Ed.), Ceramic Hard Materials, Wiley VCH, Weinheim, 2000.

[4] T.A. Scott, The influence of microstructure on the mechanical properties of polycrystalline diamond: a literature review, Adv. Appl. Ceram. 117 (3) (2018) 161–176.

[5] R.I. Todd, B. Derby, Thermal stress induced microcracking in alumina–20% SiCp composites, Acta Mater. 52 (2004) 1621–1629.

[6] R.W. Davidge, T.J. Green, The strength of two-phase ceramic/glass materials, J. Mater. Sci. 3 (1968) 629–634.

[7] J. Zhang, R. Tu, T. Goto, Densification. microstructure and mechanical properties of SiO_2–cBN composites by spark plasma sintering, Ceram. Int. 38 (2012) 351–356, https://doi.org/10.1016/j.ceramint.2011.07.013.

[8] P. Klimczyk, P. Wyżga, J. Cyboroń, J. Laszkiewicz-Łukasik, M. Podsiadło, S. Cygan, L. Jaworska, Phase stability and mechanical properties of Al_2O_3-cBN composites prepared via spark plasma sintering, Diam. Relat. Mater. 104 (2020) 107762, https://doi.org/10.1016/j.diamond.2020.107762.

[9] J.C. Garrett, I. Sigalas, M. Herrmann, E.J. Olivier, J.H. O'Connell, cBN reinforced Y-α-SiAlON composites, J. Eur. Ceram. Soc. 33 (2013) 2191–2198, https://doi.org/10.1016/j.jeurceramsoc.2013.03.014.

[10] A.-K. Wolfrum, C. Quitzke, B. Matthey, M. Herrmann, A. Michaelis, Wear behavior of diamond-silicon nitride composites sintered with FAST/SPS, Wear 396–397 (2018) 172–181, https://doi.org/10.1016/j.wear.2016.10.021.

[11] A.-K. Wolfrum, Verdichtung und Eigenschaften von Hartstoffverstärkten Siliciumnitridwerkstoffen. Ph.D. Dissertation, Technische Universität Dresden. Dresden. Germany, 2019.

[12] H.M. Irshad, B.A. Ahmed, M.A. Ehsan, T.I. Khan, T. Laoui, M.R. Yousaf, A. Ibrahim, A.S. Hakeem, Investigation of the structural and mechanical properties of micro-/nano-sized Al2O3 and cBN composites prepared by spark plasma sintering, Ceram. Int. 43 (2017) 10645–10653.

[13] H.M. Irshad, B.A. Ahmed, M.A. Ehsan, T.I. Khan, T. Laoui, M.R. Yousaf, A. Ibrahim, A.S. Hakeem, Tribological behaviour of alumina-based nanocomposites reinforced with uncoated and Ni-coated cubic boron nitride, J. Mater. Res. Technol. 8 (2019) 5066–5079.

[14] O. Fukunaga, The equilibrium phase boundary between hexagonal and cubic boron nitride, Diam. Relat. Mater. 9 (2000) 7–12, https://doi.org/10.1016/S0925-9635(99)00188-0.

[15] A.-K. Wolfrum, B. Matthey, A. Michaelis, M. Herrmann, On the stability of c-BN-reinforcing particles in ceramic matrix materials, Materials 11 (2018), https://doi.org/10.3390/ma11020255.

[16] C. Zhu, J. Lang, N. Ma, Preparation of Si–diamond–SiC composites by in situ reactive sintering and their thermal properties, Ceram. Int. 38 (8) (2012) 6131–6136.

[17] K. Hirota, M. Aoki, M. Kato, M. Ueda, Y. Nakamori, Fabrication of diamond/SiC composites using HIP from the mixtures of diamond and Si powders, Mater. Res. Proceed. 10 (2019) 190–196.

[18] Y. Liu, C. Hu, W. Feng, J. Men, L. Cheng, L. Zhang, Microstructure and properties of diamond/SiC composites prepared by tape-casting and chemical vapor infiltration process, J. Eur. Ceram. Soc. 34 (2014) 3489–3498.

[19] Z. Yang, X. He, M. Wu, L. Zhang, A. Ma, R. Liu, H. Hu, Y. Zhang, X. Qu, Fabrication of diamond/SiC composites by Si-vapor vacuum reactive infiltration, Ceram. Int. 39 (2013) 3399–3403.

[20] B. Matthey, Siliciumcarbid gebundene Diamantwerkstoffe - Herstellung. Mikrostruktur und Eigenschaften. Dissertation, Technische Universität Dresden, 2018.

[21] S. K. Gordeev. S. G. Zhukov. L. V. Danchukova. T. Ekstroem. Method of Manufacturing a Diamond-Silicon Carbide-Silicon Composite and a Composite Produced by This Method. WO9912866. 1999.

[22] S.K. Gordeev, A. Yu Ezhov, T.D. Karimbaev, S.B. Korchagina, M.A. Mezentsev, New materials for machinery engineering silicon carbide reinforced with diamond particles, Kompozity i Nanostruktury 7 (2) (2015) 61–71.

[23] S.K. Gordeev, S.G. Zhukov, L.V. Danchukova, T.C. Ekstrom, Low-pressure fabrication of diamond–SiC–Si composites, Inorg. Mater. 37 (6) (2001) 579–583.

[24] K. Mlungwane, I. Sigalas, M. Herrmann, The development of a diamond silicon carbide composite material, Ind. Diam. Rev. 65/4 (2005) 62–65.

[25] M. Herrmann, B. Matthey, S. Höhn, I. Kinski, D. Rafaja, A. Michaelis, Diamond-ceramics composites - new materials for a wide range of challenging applications, J. Eur. Ceram. Soc. 32/9 (2012) 1915–1923.

[26] B. Matthey, S. Kunze, M. Hörner, B. Blug, M. van Geldern, A. Michaelis, M. Herrmann, SiC-bonded diamond materials produced by pressureless silicon infiltration, J. Mater. Res. 32/17 (2017) 3362–3371.

[27] B. Matthey, S. Höhn, A.-K. Wolfrum, U. Mühle, M. Motylenko, D. Rafaja, A. Michaelis, M. Herrmann, Microstructural investigation of diamond-SiC composites produced by pressureless silicon infiltration, Europ. Ceram. Soc. 37 (2017), https://doi.org/10.1016/j.jeurceramsoc.2016.12.008 1917-192.

[28] G. Jungnickel, D. Porezag, T. Frauenheim, M.I. Heggie, W.R.L. Lambrecht, B. Segall, J.C. Angus, Graphitization effects on diamond surfaces and the diamond/graphite interface, Phys. Status Solidi 154 (1) (1996) 109–125.

[29] Y. Zhang, C.-Y. Hsu, P. Karandikar, C. Ni, Interfacial zone surrounding the diamond in reaction bonded diamond/SiC composites: interphase structure and formation mechanism, Europ. Ceram. Soc. 39 (2019) 5190–5196, https://doi.org/10.1016/j.jeurceramsoc.2019.08.019.

[30] M. Sebastiani, K.E. Johanns, E.G. Herbert, Measurement of fracture toughness by nanoindentation methods: recent advances and future challenges, Curr. Opin. Solid State Mater. Sci. 19 (2015) 324–333.

[31] V. Maier, K. Durst, J. Mueller, B. Backes, H. Höppel, M. Göken, Nanoindentation strain-rate jump tests for determining the local strain-rate sensitivity in nanocrystalline Ni and ultrafine-grained Al, J. Mater. Res. 26 (2011) 1421–1430, https://doi.org/10.1557/jmr.2011.156.

[32] J. Ast, M. Ghidelli, K. Durst, M. Göken, M. Sebastiani, A review of experimental approaches to fracture toughness evaluation at the micro-scale, Mater. Des. 173 (2019). Article 107762.

[33] J. Buchinger, L.Öffler J. Ast, A. Wagner, Fracture properties of thin film TiN at elevated temperatures, Mater. Des. 194 (2020). Article 108885.

[34] J. Ast, T. Przybilla, V. Maier, K. Durst, Microcantilever bending experiments in NiAl - evaluation, size effects, and crack tip plasticity, J. Mater. Res. 29 (2014) 2129–2140.

[35] J.P. Best, J. Zechner, J.M. Wheeler, Small-scale fracture toughness of ceramic thin films: the effects of specimen geometry, ion beam notching and high temperature on chromium nitride toughness evaluation, Phil. Mag. 96 (2016) 3552–3569, https://doi.org/10.1080/14786435.2016.1223891.

[36] K. Matoy, T. Detzel, M. Müller, C. Motz, G. Dehm, Interface fracture properties of thin films studied by using the micro-cantilever deflection technique, Surf. Coating. Technol. 204 (2009) 878–881.

[37] G. Dehm, B.N. Jaya, R. Raghavan, C. Kirchlechner, Overview on micro- and nanomechanical testing: new insights in interface plasticity and fracture at small length scales, Acta Mater. 142 (2018) 248–282.

[38] J.P. Best, J. Wehrs, M. Polyakov, M. Morstein, J. Michler, High temperature fracture toughness of ceramic coatings evaluated using micro-pillar splitting, Scripta Mater. 162 (2019) 190–194.

[39] A. Naughton-Duszová, T. Csanádi, R. Sedlák, P. Hvizdoš, J. Dusza, Small-Scale mechanical testing of cemented carbides from the micro- to the nano-level: a review, Metals 9 (2019) 502, https://doi.org/10.3390/met9050502.

[40] Y. Zhang. C. Hsu. T. Wang. P. Karandikar. C. Ni. Mechanical and Thermal Characteristics of Interfaces and Defects in diamond/SiC Composites (Invited). ICACC-S4-030-2020.

[41] C.-Y. Hsu, Y. Zhang, Y. Xie, F. Deng, P. Karandikar, J.Q. Xiao, C. Ni, In-situ measurement of SiC/Si interfacial tensile strength of reaction bonded SiC/Si composite, Compos. B Eng. 175 (2019) 107–116, https://doi.org/10.1016/j.compositesb.2019.107116.

[42] T.A. Scott, DPhil Thesis, University of Oxford, 2020.

[43] J.D. Clayton, M. Guziewski, J.P. Ligda, R.B. Leavy, J. Knap, A multi-scale Approach for phase field modeling of ultra-hard ceramic composites, Materials 14 (2021) 1408, https://doi.org/10.3390/ma14061408 10.3390/ma14061408.

[44] M. Herrmann, L. Adloff, B. Matthey, T. Gestrich, Oxidation behaviour of silicon carbide bonded diamond materials, Open Ceram. 2 (2020) 100017, https://doi.org/10.1016/j.oceram.2020.100017.

[45] B. Matthey, T. Pirling, M. Herrmann, J. Schreiber, Determination of bulk residual stresses in superhard diamond-SiC materials, J. Eur. Ceram. Soc. 40 (2020) 1035–1042, https://doi.org/10.1016/j.jeurceramsoc.2019.11.055.